University of Plymouth

PEARL **https://pearl.plymouth.ac.uk**

01 University of Plymouth Research Outputs University of Plymouth Research Outputs

2017-01-30

Wave simulation for the design of an innovative quay wall: the case of Vlore Harbour

Antonini, Alessandro

http://hdl.handle.net/10026.1/8678

10.5194/nhess-17-127-2017
Natural Hazards and Earth System Sciences
Copernicus GmbH

All content in PEARL is protected by copyright law. Author manuscripts are made available in accordance with publisher policies. Please cite only the published version using the details provided on the item record or document. In the absence of an open licence (e.g. Creative Commons), permissions for further reuse of content should be sought from the publisher or author.

Nat. Hazards Earth Syst. Sci., 17, 127–142, 2017
www.nat-hazards-earth-syst-sci.net/17/127/2017/
doi:10.5194/nhess-17-127-2017
© Author(s) 2017. CC Attribution 3.0 License.

Natural Hazards and Earth System Sciences Open Access EGU

Wave simulation for the design of an innovative quay wall: the case of Vlorë Harbour

Alessandro Antonini[1], **Renata Archetti**[2,3,4], **and Alberto Lamberti**[2,4]

[1]Coastal, Ocean and Sediment Transport Research Group – Plymouth University – Marine Building, Drake Circus, Plymouth, Devon, PL4 8AA, UK
[2]DICAM, University of Bologna, Bologna, 40136, Italy
[3]CONISMA, Consorzio Nazionale Interuniversitario per le Scienze del Mare, Rome 00196, Italy
[4]CIRI Edilizia e Costruzioni, University of Bologna, Bologna, 40100, Italy

Correspondence to: Renata Archetti (renata.archetti@unibo.it)

Received: 14 May 2016 – Published in Nat. Hazards Earth Syst. Sci. Discuss.: 13 June 2016
Revised: 5 October 2016 – Accepted: 27 October 2016 – Published: 30 January 2017

Abstract. Sea states and environmental conditions are basic data for the design of marine structures. Hindcasted wave data have been applied here with the aim of identifying the proper design conditions for an innovative quay wall concept. In this paper, the results of a computational fluid dynamics model are used to optimise the new absorbing quay wall of Vlorë Harbour (Republic of Albania) and define the design loads under extreme wave conditions. The design wave states at the harbour entrance have been estimated analysing 31 years of hindcasted wave data simulated through the application of WaveWatch III. Due to the particular geography and topography of the Bay of Vlorë, wave conditions generated from the north-west are transferred to the harbour entrance with the application of a 2-D spectral wave module, whereas southern wave states, which are also the most critical for the port structures, are defined by means of a wave generation model, according to the available wind measurements. Finally, the identified extreme events have been used, through the NewWave approach, as boundary conditions for the numerical analysis of the interaction between the quay wall and the extreme events. The results show that the proposed method, based on numerical modelling at different scales from macro to meso and to micro, allows for the identification of the best site-specific solutions, also for a location devoid of any wave measurement. In this light, the objectives of the paper are two-fold. First, they show the application of sea condition estimations through the use of wave hindcasted data in order to properly define the design wave conditions for a new harbour structure. Second, they present a new approach for investigating an innovative absorbing quay wall based on CFD modelling and the NewWave theory.

1 Introduction

The development of global trade and ship transportation often requires that the existing docks must be upgraded, consolidated or enlarged in order to face effectively the increasing demand of people and freight traffic. With such aims, quays built above absorbing rubble mounds can be used to enlarge or rebuild structures in the existing docks. Generally, the rubble mound structures assure low reflection in the port basins, which is very important for mooring and manoeuvring but they lead to the construction of very wide superstructures. The construction of these superstructure is not always possible due to the restrictions in the available spaces and financial sources. The use of vertical walls as berthing structures is an alternative often used in port areas: in fact this kind of solution represents a compromise between the simplicity of construction and the need to occupy a small area. Nevertheless, vertical quay walls present a drawback of undesirable high-wave reflection into the port areas. A low-reflecting quay might sort out the reflection issue in port areas by means of porous or open structures that dissipate part of the incident wave energy. Therefore, several different vertical dissipative solutions have been proposed during the last decades as a result of research studies from all over the world.

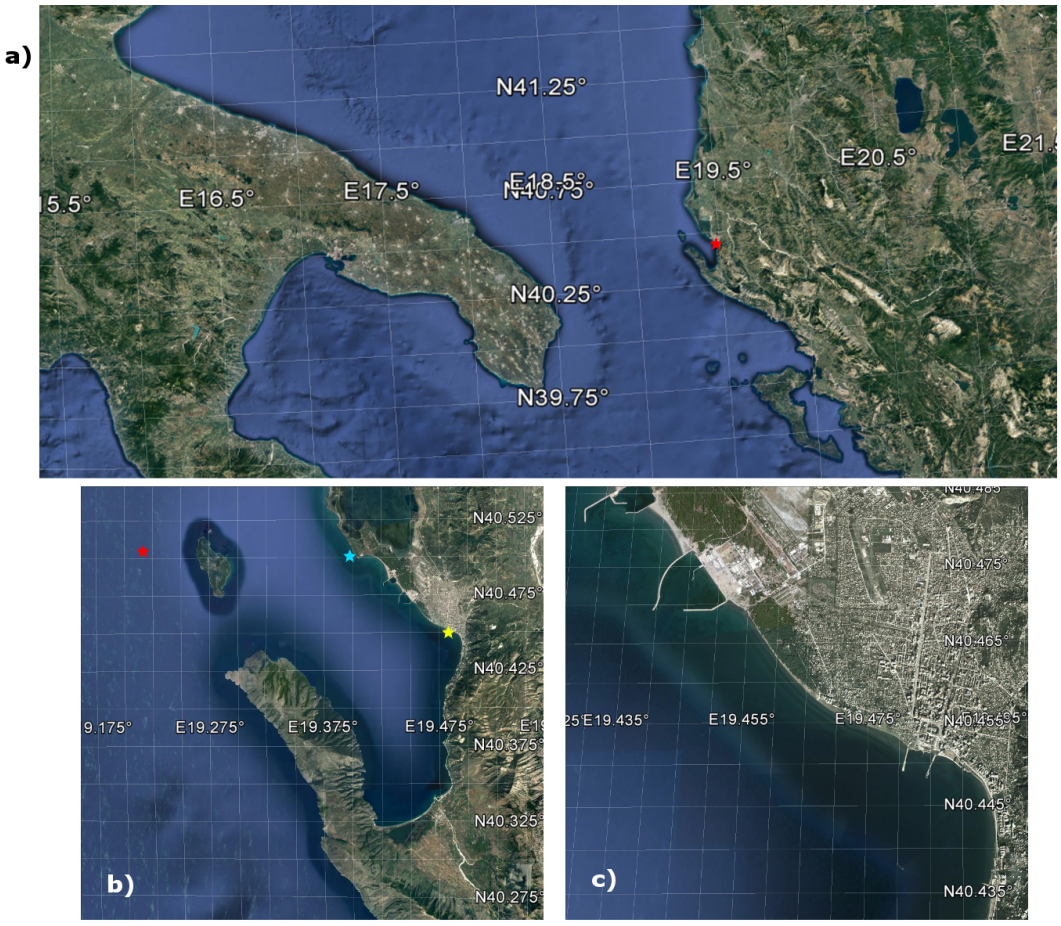

Figure 1. **(a)** Location of Vlorë, **(b)** wave hindcast extraction point (red star), Vlorë Harbour (yellow star), wind data measurement point (blue star); **(c)** view of Vlorë Harbour.

The availability of wave data is necessary for pursing the design of innovative harbour parts, as the quays and docks. For several remote locations direct measurements are not always available and series of hindcasted waves are necessary for defining the proper conditions at the harbour entrance. The most common operative wave models are WaveWatch III, WAM and SWAN (The WAMDI Group, 1988; Monbaliu et al., 2000; Booij and Holthuijsen, 1999).

The WaveWatch III model (http://polar.ncep.noaa.gov/waves/wavewatch/wavewatch.shtml), developed by the National Weather Service (NWS) and National Oceanic and Atmospheric Administration (NOAA) is operational at DICCA, University of Genoa. The model covers the whole of the Mediterranean basin with a resolution equal to 0.1° (Sartini et al., 2014, 2015a, b). The model chain, extensively validated by Mentaschi et al. (2015a), is forced with the National Centers for Environmental Prediction Climate Forecast System Reanalysis data at 0.5° resolution. In this paper, the design wave conditions are estimated by means of extreme wave analysis applied to the numerical results. An extreme event analysis can be based on different methodologies (Mazas et al., 2014; Masina et al., 2015) while the historic and most used design approach leads to the use of the peak over threshold technique to select sample data (Mathiesen et al., 1994; Garcia-Espinel et al., 2015).

To attenuate wave reflection various structures have been designed, Jarlan-type structures (Jarlan, 1961) being the most widely used. However, all the existing absorbing solutions for vertical maritime structures have the drawback that their exiguous efficacy reduces the reflection of low-frequency waves (i.e. wave periods larger than 25 s). To overcome this technical problem, the design of a vertical structure can be based on a multi-cell circuit concept which is considered to be especially effective to reduce the wave reflection of wind waves and oscillations associated with intense storms and resonance waves in port basins (Medina et al., 2010). Furthermore, Altomare and Gironella (2014), Matteotti (1991) and Faraci et al. (2012) investigated, by means of physical model tests, several quay walls consisting of prefabricated caissons with frontal openings and internal rubble mounds. In the paper, a similar solution is shown, consisting of a retaining wall realised by a combi-wall structure and a frontal

opening with internal rubble mounds. Throughout the paper, the use of hindcasted data are used to properly define the design conditions at the entrance of Vlorë Harbour, while the quay wall structure is investigated using CFD simulations (CD-ADAPCO, 2013; Lamberti et al., 2014).

2 Site description

The city of Vlorë, in the Republic of Albania, is located on a coastal plain in the north-eastern part of the bay. The bay is approximately 17 km long and 10 km wide with a depth that reaches 55 m. It is open to the Adriatic Sea through the north-western side and is bordered by tall and craggy mountain peaks on the southern and western sides. The bay is also partially protected from the swells coming from the north-west by the presence of Sazan Island, located at the northern part of the bay, and by the shallow water next to the mouth of the Vjosa River (see Fig. 1a). The investigated port is located in the small northern stretch of the coast in the inner part of the bay. The location of the new harbour is presented in Fig. 1b with a yellow star.

In the surrounding area some port infrastructures are already presented. Some of them are still working and others are disused. The facilities include an offshore berth for tankers called New Port and the historic Old Port of Vlorë. The harbour under investigation is characterised by the presence of two piers, as shown in Fig. 1c, called the west wharf and east pier. The first is primarily intended for docking ferry passengers while the second is used for berthing cargo vessels.

3 Design wave conditions

No measured wave data are available for the Bay of Vlorë; therefore wave climate is defined as 31 years (1999–2010) of hindcasted wave data supplied by the University of Genova (Sartini et al., 2015a; Mentaschi et al., 2015b). The extraction point (red star in Fig. 1b) is selected in order to represent the wave climate outside the gulf. The wave rose at the extraction point is shown in Fig. 2.

Two main directional sectors are evident: the first sector between −120 and +40° N, associated with the axis direction of the Adriatic, and the second sector between 160 and 200° N, providing information on southern waves. The dominant wave condition is related to the sector between 155 and 170° N, whereas the maximum occurrence frequency, i.e. 15 %, of the northern events is related to 300° N. The maximum northerly wave height is equal to 5.75 m, with a peak period of 10 s.

Due to the particular geography and topography of the bay, southern hindcasted wave data are not representative of the actual conditions in the vicinity of the port. Consequently, the definition of southern wave states (S–SW) requires other

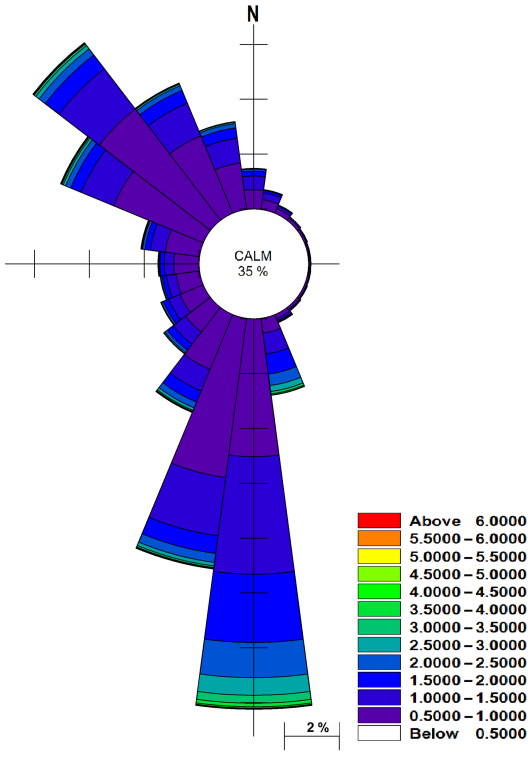

Figure 2. Wave rose at the entrance of Bay of Vlorë (coord. 40°30′ N, 19°12′ E.)

data sources like wind measurements to be partially available inside the bay.

In order to define the design wave conditions at the harbour entrance, two different approaches have been undertaken according to the propagation direction. For both the interested directions, the exercise and extreme conditions are defined according to return periods of 2 and 100 years, respectively. A return period event of 2 years is accounted for by the limit of ordinary operation, i.e. the limit condition for which there should not be any malfunction of the harbour infrastructure. A return period event of 100 years is considered for the design condition of the structures, i.e. the event for which only the structures should resist. The northern wave conditions are established by the extreme wave analysis, performed on the hindcasted wave data. The southern wave conditions are estimated by applying the wave generation model, Mike21-SW on the Bay of Vlorë, by imposing a local wind intensity with $T_R = 2$ years and $T_R = 100$ years.

3.1 Design waves from NW

The peak over threshold method (POT) has been applied to the northern storm time series (N–NW) in order to select independent storm peaks. The technique is a well-established statistical approach, based on the following steps: (i) the application of a proper threshold, (ii) the selection of homogeneous independent events and peaks which exceed the

selected threshold, (iii) the identification of the probability model that best represents the exceedances and (iv) a determination of values within a given return period.

The POT analysis has been applied to the wave data, providing the results illustrated in Fig. 3, in which the empirical frequency histogram and cumulative distribution function (PDF and CDF) are given along with the corresponding Gumbel distribution with the best-fit scale parameter (σ) and location parameter (μ) equal to 0.58 (95 % lower and upper bounds parameter fitting: 0.55–0.61), 2.51 (95 % lower and upper bounds parameter fitting: 2.48–2.55), respectively. The threshold used to define an individual storm has been established according to Boccotti's method (Boccotti, 2000). The method is based on the identification of a wave height threshold, namely 1.5 times the annual average H_{Sy}, that is equal to 1.0 m for the available wave data: the adopted threshold value is therefore equal to 1.50 m. The application of the described approach led to the detection of 355 independent events from the direction −120 to +40° N. The northern sector is between 285 and 345° N. It is worth remarking that the significant wave height (H_{STR30}) of the estimated 30-year return period ($T_R = 30$ years) is equal to 5.8 m, in good agreement with the maximum hindcasted wave height equal to 5.75 m. The resulting values of H_S for the selected wave heights are listed in Table 1. The analyses have provided the significant wave height (H_s) and the mean peak period (T_p), with values given in Table 1 with reference to return periods of 2 years and 100 years. The mean peak periods associated with the predicted significant wave heights have been calculated using a scatter plot of simulated peak periods versus significant wave height as proposed by Viselli et al. (2015) and Schweizer et al. (2016). The parameters a and b in Eq. (1). turn out to be equal to 2.36 (0.30, 4.42) and 0.72 (0.43, 1.01), respectively; values in parentheses indicate the lower and upper bounds of the 95 % confidence interval.

$$T_p = a \cdot H_s^b \quad (1)$$

The numerical model Mike 21-SW was then applied to propagate such conditions from the offshore location to the entrance of the port. The spectral wave model simulates the growth, decay and transformation of wind-generated waves. MIKE21-SW is a third-generation spectral wave model, as it does not require any parameterisation of either the spectral or the directional distribution of power. The modelled physical processes comprise: (a) energy source-dissipation processes (wind driven interactions with atmosphere, dissipation through wave breaking and white-capping and bottom friction-induced dissipation), (b) non-linear energy transfer conservative processes (resonant quadruplet interactions, triad interactions) and (c) wave propagation-related processes (wave propagation due to the wave group, depth induced refraction, shoaling). The models compute the evolution of wave action density by solving the action balance equation as described by Booij et al. (1999). Numerical propagation has been completed by means of unstructured triangular meshes as recently applied by Samaras et al. (2016) and Gaeta et al. (2016). The adopted bathymetric and shoreline data result from the digitisation of nautical charts acquired from the Italian Hydrographic Institute. The triangular mesh dimension is homogeneous over the entire domain, resulting in a mesh of 102 995 elements with a mean dimension of 600 m^2. The adopted grid is shown in Fig. 4.

Table 1. Interpretation of extreme events using the hindcasted northern wave data at the selected location off the Bay of Vlorë.

	H_s [m]	T_p [s]	Dir [° N]
$T_R = 2$ years	4.40	8.5	310
$T_R = 100$ years	6.85	11.0	310

Table 2. Wave conditions extracted at the harbour entrance (UTM coord. 371221° E, 4478470° N).

	H_s [m]	T_p [s]	Dir [° N]
$T_R = 2$ years	1.00	8.5	260
$T_R = 100$ years	1.70	11.0	265

Wave fields of H_{TR2} and H_{TR100} are presented in Figs. 5 and 6, in which reduction of the wave height due to the shoaling is shown. The design conditions at the harbour entrance at 13.5 m water depth (UTM coord. 371221° E, 4478470° N; Fig. 6) are shown in Table 2.

3.2 Design waves from *S*

Southerly design wave conditions are not easily estimated, as direct measurements of waves inside the Bay of Vlorë were not available and wind data were also relatively scarce. Such conditions, which are also the most critical for the port structures, were defined by a wave generation model, MIKE21-SW, after an empirical extrapolation of the wind intensity based on 2 years of measured data.

The approach is well known and shortly summarised here: wind-wave generation is the process by which the wind transfers energy into the water body, generating waves. The wind input is based on Janssen's (1989, 1991) quasi-linear theory of wind-wave generation, in which the momentum transfer from the wind to the sea not only depends on the wind stress, but also on the sea state itself. The source function describing the dissipation due to white capping is based on the theory of Hasselmann et al. (1985) and Janssen (1989), while the source function describing the bottom-induced wave breaking is based on the well-proven approach of Battjes and Janssen (1978) and Eldeberky and Battjes (1996). More details on the wave generation model are provided in the DHI Manual (2011). The generation model was forced with $T_R = 2$ and $T_R = 100$ wind intensity values (see Table 3).

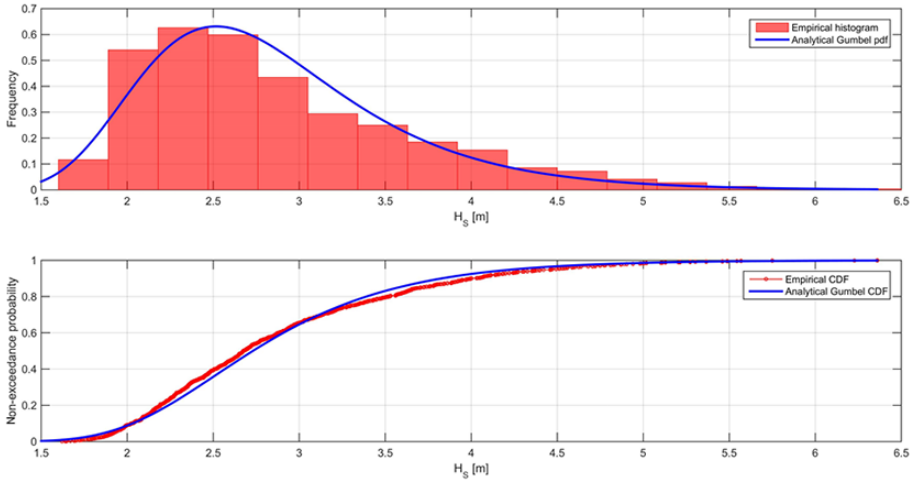

Figure 3. Interpretation of the wave data at the study area: **(a)** empirical and analytical PDF and **(b)** empirical and analytical CDF for the identified peak values.

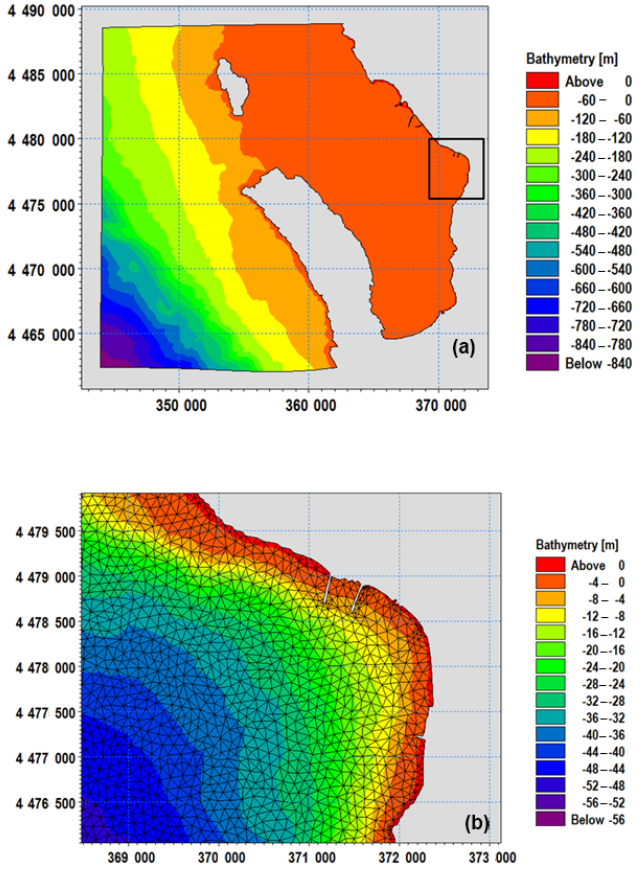

Figure 4. Bathymetry of the wave model **(a)** and close-up of the bathymetry and mesh at the harbour entrance area **(b)**.

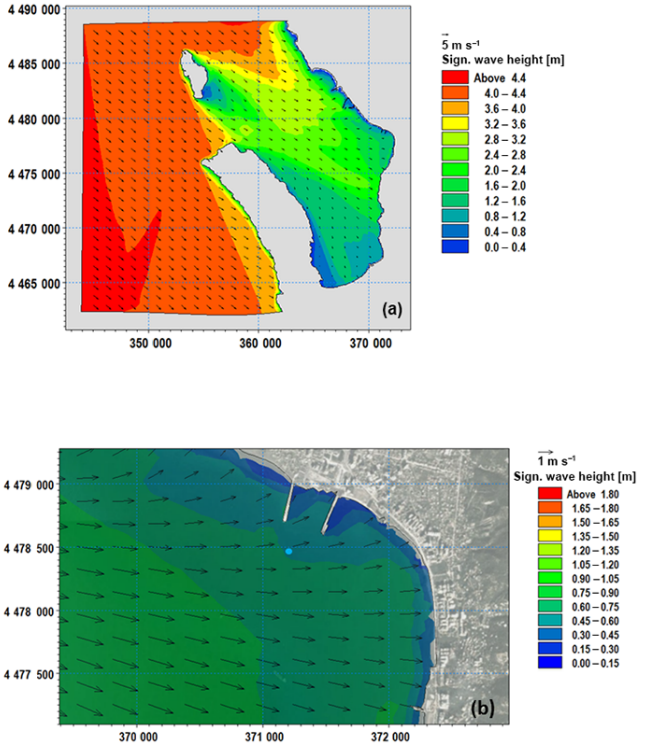

Figure 5. Wave field for the design wave condition $H_S = 4.40$ m, $T_p = 8.5$ s, Dir = 310° N. **(a)** Entire domain, **(b)** harbour entrance. The blue bullet is the extraction point location; its UTM coordinates are 371221° E, 4478470° N.

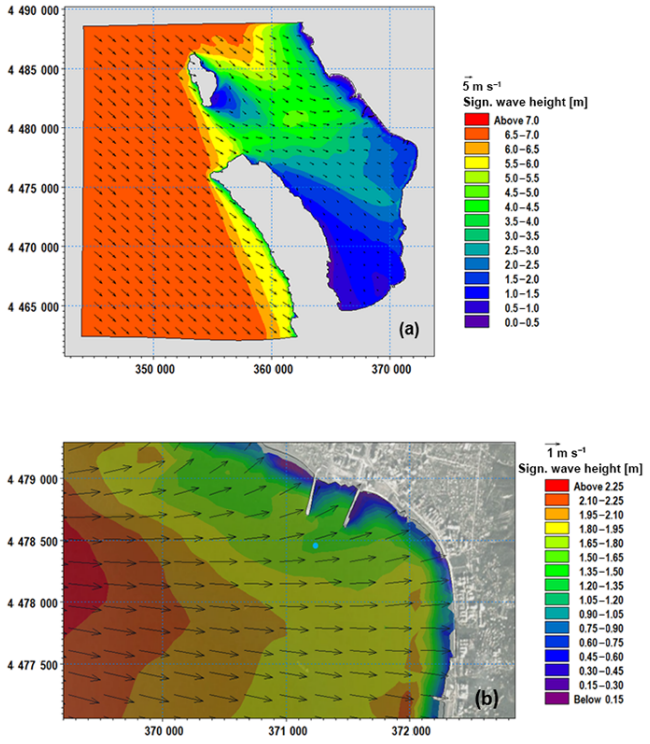

Figure 6. Wave field for the design wave condition $H_S = 6.85$, $T_p = 11$, Dir = 310° N. **(a)** Entire domain, **(b)** harbour entrance. The blue bullet is the extraction point location; its UTM coordinates are 371221° E, 4478470° N.

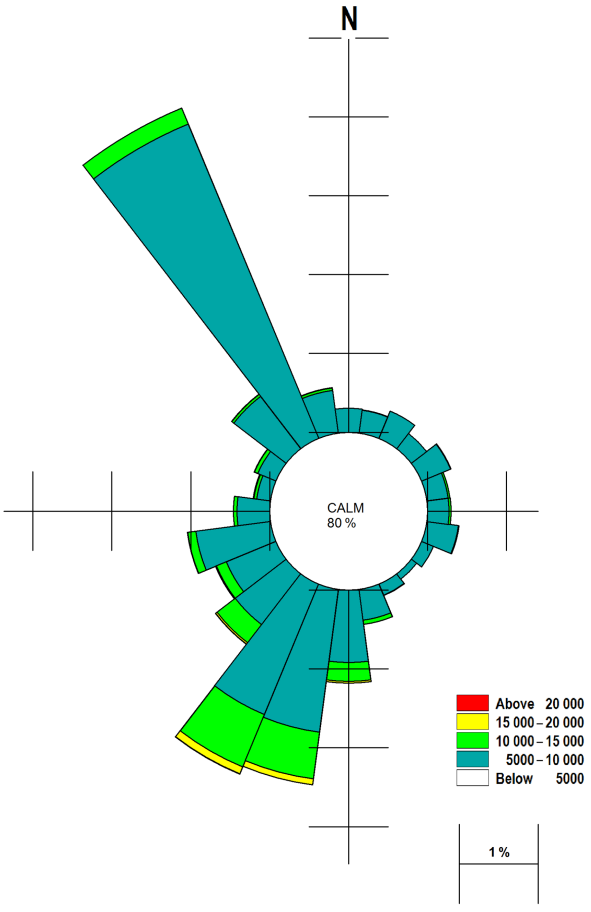

Figure 7. Wind rose (July 2006–August 2008).

Table 3. Wind conditions used as input to the MIKE21-SW wave generation model, Lamberti et al. (2015).

	U [m s^{-1}]	Dir [° N]
$T_R = 2$ years	22	215
$T_R = 100$ years	41	215

Wind data measurements were supplied by SIAP-MICROS s.r.l., the anemometer was installed on the Albania coast at point of coordinate 40° 30′51.98″ N, 19° 23′36.69″ E, presented on Fig. 1b with a blue star; the resulting wind rose is shown in Fig. 7. The measurement protocol followed the standard, measuring every 10 min. The instrument has been working for 2 years (July 2006–August 2008). The statistical analysis of the data was preceded by a quality control check of all data in order to remove the outliers and to interpolate over small data gaps that may be present. Overall, the corrected data were of sufficient quality, with less than 3 % of the data removed as outliers or unacceptable values; Belu and Koraicn (2009). The highest measured value is equal to 22.8 m s^{-1}, while a gust reduction factor equal to 0.96 is applied in order to define the effective wind velocity (El-Hawary, 2000). The minimum effective southern wind duration for the Bay of Vlorë is estimated through the SMB (Sverdrup–Munk–Bretschneider) method and is equal to 1 h for an effective fetch of 10 km length (US Army corps of engineers, 1984). Under the hypothesis of a constant difference between wave heights characterised by two consecutive return periods of different orders of magnitude (i.e. $\Delta H_s = (H_{sTR10} - H_{sTR1}) = (H_{sTR100} - H_{sTR10}) = 1.35$ m) the centennial wave state was estimated to be equal to a significant wave height of 3.8 m and peak period of 6.1 s. Within the inverse SMB procedure, the centennial wind intensity is estimated to be equal to 41 m s^{-1}.

It should be said that the dearth of data and the empirical nature of the stated procedure might produce uncertainty of the calculated values. Therefore, in order to validate the adopted method, the wave field forced by the mentioned wind conditions was generated through the wave generation model of the MIKE 21 SW. The results are presented in Table 3 and in Figs. 8 and 9, while the extracted wave conditions at the harbour entrance are presented in Table 4. The final results of the design waves are a set of four wave conditions for the two incoming wave directions (i.e. north-west and south-west) and the two return periods (i.e. 2 and 100 years); Table 4.

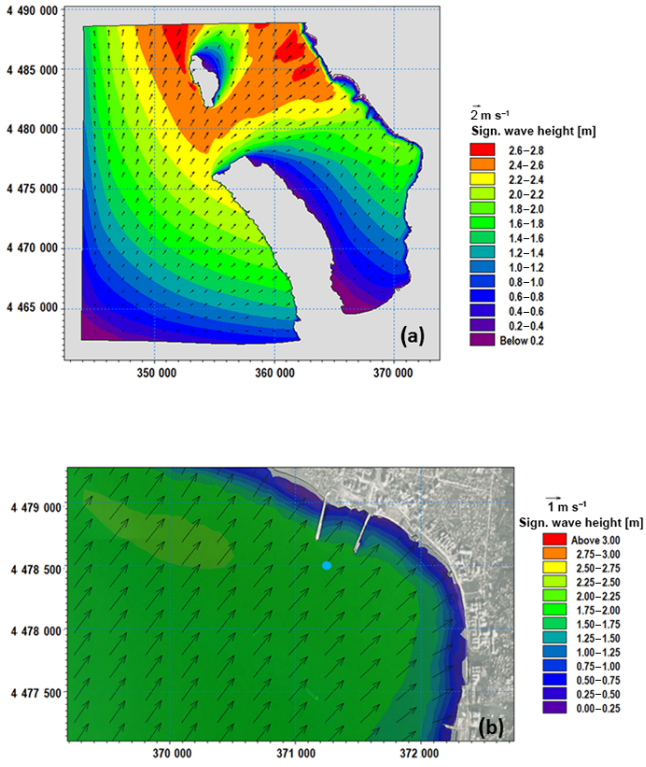

Figure 8. Wave field for the design wave condition generated by southern wind $U = 22\,\mathrm{m\,s^{-1}}$, Dir 215° N, $T_R = 2$ years. **(a)** Entire domain, **(b)** harbour entrance. The blue bullet is the extraction point location; its UTM coordinates are 371221° E, 4478470° N.

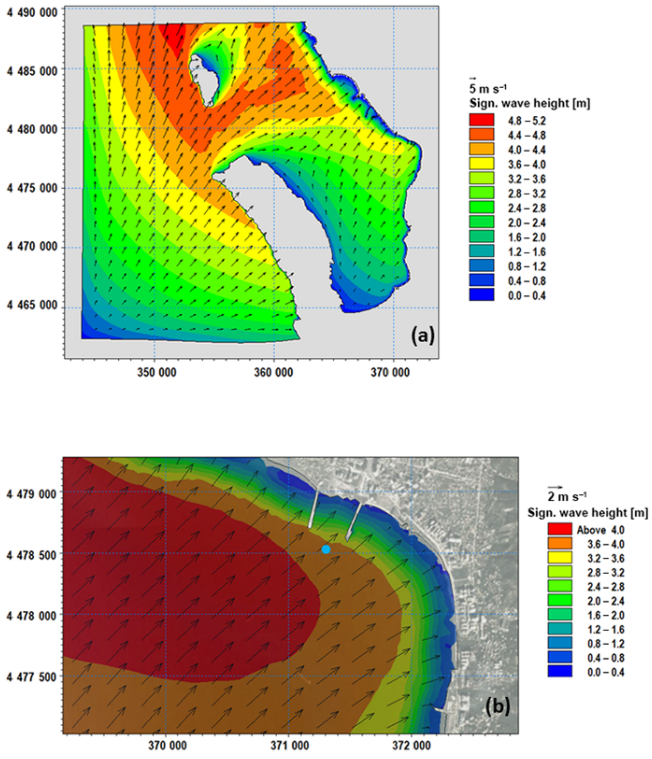

Figure 9. Wave field for the design wave condition generated by southern wind $U = 41\,\mathrm{m\,s^{-1}}$, Dir 215° N, $T_R = 100$ years. **(a)** Entire domain, **(b)** harbour entrance. The blue bullet is the extraction point location; its UTM coordinates are 371221° E, 4478470° N.

Table 4. Selected design wave states.

Wave no.	T_R (years)	H_s (m)	T_p (s)	Length (m)	Dir (° N)
1	2	1.0	8.5	85.5	260
2	100	1.70	11.0	117.0	265
3	2	1.8	4.5	31.3	215
4	100	3.8	6.1	53.4	215

4 CFD modelling of the quay wall

The quay wall structure, consisting of steel sheet-pile foundation and an absorbing wave chamber, is investigated through CFD model by means of the commercial code STAR-CCM+, already widely used for design, as in Antonini et al. (2016a, b, c). The innovative design is presented in Fig. 10, while the optimum site-specific geometry is defined through the comparison of three geometries. The changes made during the analysis are related to the following:

1. the length of the absorbing wave chamber;
2. the extension of the gap between front reflective surface and free surface;
3. the arrangement of the armour slope inside the cell.

The aim of the site-specific absorbing quay wall design is the maximisation of the wave energy dissipation according to the exercise wave condition (described in Table 4). The goal is reached using a cell length as close as possible to the quarter of the considered wavelength; therefore only a single wave state is adopted to optimise the geometry of the cell. In this light, the optimisation of the absorbing cell is carried out according to the exercise wave condition from the south-west, i.e. wave no. 3 ($H_s = 1.80$ m, $H_{max} = 3.2$ m, $T_p = 4.5$ s, $T_s = 4.2$ s), while for waves no. 1 and 4 the performances of the optimised quay wall are investigated.

The chamber width, which will be varied through the design phase, is filled with a rubble mound in order to induce dissipation due to the breaking wave. With an aim to not affect the rubble mound stability, the top of the slope is always kept under the seawater level according to three main restrictions: (i) the design diameter of the natural stone, (ii) the maximum allowed steepness and (iii) the limited chamber length. The geometry of structure 1 has a cell length equal to 5.47 m and the frontal reflective surface extends from −7.5 to −2.5 m. The armour slope extends from the front sheet pile up to the rear beam installed on top of rear sheet pile, with a nominal diameter (D_{N50}) equal to 1.0 m, (Fig. 11a).

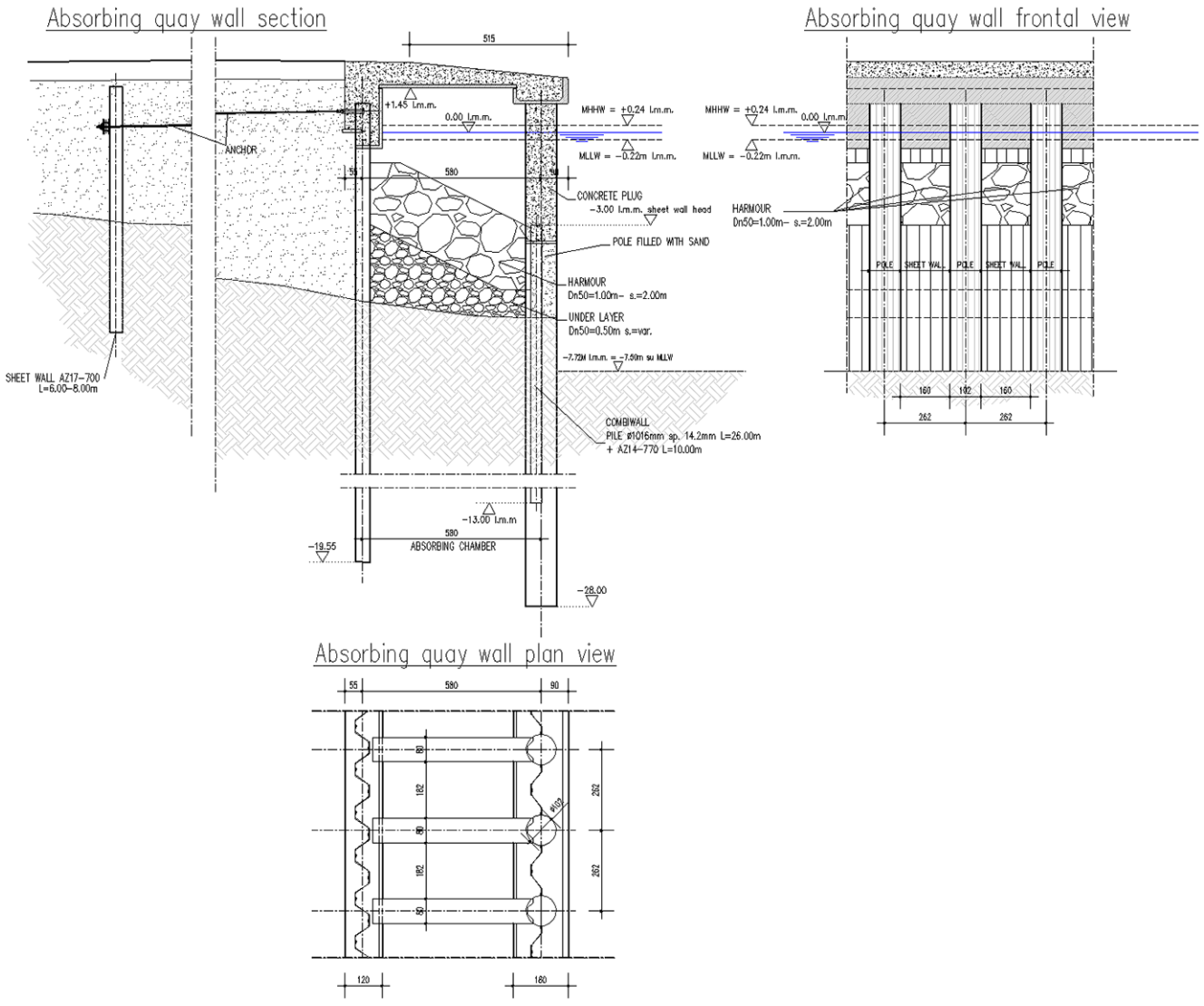

Figure 10. Absorbing quay wall section, plan and frontal views.

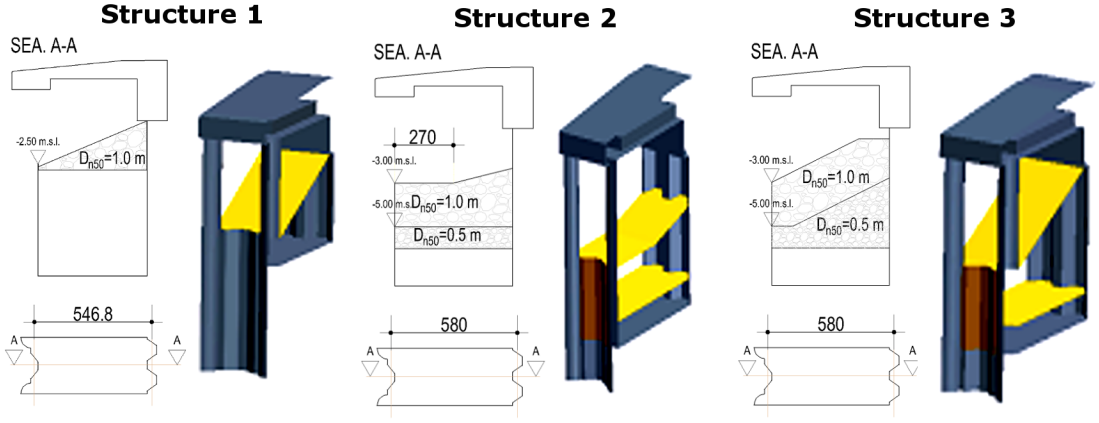

Figure 11. Simplified section and cad representation of the tested structures.

The geometry of structure 2 has cell length equal to 5.80 m and the front reflective surface extends from −7.5 to −3.0 m. The armour slope extends horizontally from the frontal sheet pile up to 2.70 m inside the cell where a slope of 1 : 4 reaches the rear sheet pile and the nominal diameter of the stones is 1.0 m. An underlayer with a nominal diameter of 0.50 m is designed in order to separate the rocks and the bottom sand (Fig. 11b). The geometry of structure 3 presents the same geometrical characteristics of structure 2 in terms of length and depth of the cell but there are some differences in the arrangement of the armour slope, which extends from the frontal sheet pile up to the rear one with a slope equal to 1 : 2. The stone nominal diameter is 1.0 m. (Fig. 11c).

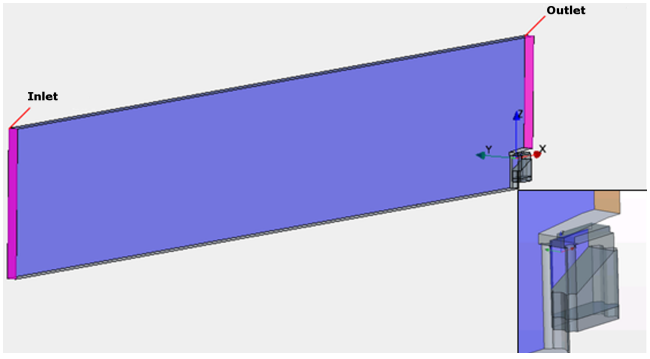

Figure 12. Domain, boundary conditions and structure details. Tank inlet is the velocity inlet boundary, Tank outlet is the pressure outlet boundary.

4.1 Modelling set-up

A $k-\omega$ SST (shear stress transport) turbulence model (Menter, 1994) is applied with a two-layer all $y+$ wall treatment model, and a second order implicit scheme was utilised for time marching. The transient SIMPLE algorithm is applied to linearise the equations and to achieve pressure–velocity coupling. A volume of fluid (VOF) method is applied to describe the free surface. The calculation is performed on a fixed grid and free surface interface orientation and shape are calculated as a function of the volume fraction of the respective fluid within a control volume.

A right-handed Cartesian coordinate system is located at the intersection between frontal structure surface, the undisturbed water surface and the medium vertical section of the domain. The longitudinal x axis points towards the outlet boundary, the z axis is vertical and points upwards, and the undisturbed free surface is the plane $z = 0$ (Fig. 12).

The domain region is 2.62 m wide ($-1.31\,\text{m} \le y \le 1.31\,\text{m}$, i.e. structure pile centre to pile centre distance), 38.75 m high ($-7.75\,\text{m} \le z \le 31.0\,\text{m}$) and its length varies according to the simulated wave group length (λ_g) (i.e. $-3/4\lambda_g \le x \le 6$), while the seabed is given 7.5 m below the mean water surface. A superposition of linear wave velocity profile is specified at the up-wave boundary in order to generate an extreme focused wave group at the structure location.

Four boundary conditions have been used to describe the fluid field at the domain bounds. They involve (i) a no-slip wall, (ii) a velocity inlet, (iii) a pressure outlet and (iv) a symmetry plane condition. The no-slip wall boundary condition represents an impenetrable, no-slip condition for viscous flow and such a boundary is used to describe the structure surface and the bottom ($z = -7.5\,\text{m}$). The velocity inlet boundary represents the inlet of the domain at which the flow velocity is known according to the required wave profile. This condition is used to model the up-wave boundary at $x = -3/4 \cdot \lambda_g$ and the top ($z = 31.0\,\text{m}$) of the domain. Lateral boundaries ($y = -1.31$ and $y = 1.31\,\text{m}$) are defined by means of symmetry planes. The pressure outlet boundary is a flow outlet boundary for which the pressure is specified and the proposed model adopts the condition of a calm water surface. Such a status is specified at the boundary above the structure ($x = 6\,\text{m}$) only for the air phase.

4.1.1 Modelling of the armour slope

The proposed armour slopes within the absorbing cell are modelled through the insertion of two solids communicating with the fluid field. By means of these volumes, dissipations due to the inertial and viscous forces are imposed by means of two coefficients. These two terms were subjected to many investigations as demonstrated by several authors (Burcharth and Andersen, 1995; Cruz et al., 1997; Engelund, 1953), who proposed different methods to calculate them according to the size and type of the modelled element. According to the Burcharth's method and considering the armour design condition, the adopted values are $6.4\,\text{kg}\,\text{m}^{-3}\,\text{s}^{-1}$ for viscous dissipation coefficient and $1221\,\text{kg}\,\text{m}^{-4}$ for the inertial coefficient, while for the underlayer, the adopted values are $26\,\text{kg}\,\text{m}^{-3}\,\text{s}^{-1}$ for viscous dissipation coefficient and $2440\,\text{kg}\,\text{m}^{-4}$ for the inertial one. The porosity value is assumed to be 0.38 and is kept constant for the porous domains.

4.1.2 Simulated wave conditions

Three different wave conditions have been simulated with two characteristics of exercise conditions (wave no. 1 and wave no. 3 in Table 4) and one dealing with extreme conditions (wave no. 4 in Table 4). We assume that the modelling of extreme condition from the north-west (i.e. wave no. 2) is not necessary as the wave state is significantly less intense than the southern one, as highlighted in the wave climate study. The wave groups are generated by a superposition of eight linear components, each of them characterised by its own amplitude, period and phase. The input signals are calculated according to the Boccotti or NewWave theories; Boccotti (1983), Boccotti et al. (1993) and Tromans et al. (1991). The procedure allows us to define an extreme focused wave group coherent with a random sea state described by a spectral distribution. In this study a Jon-

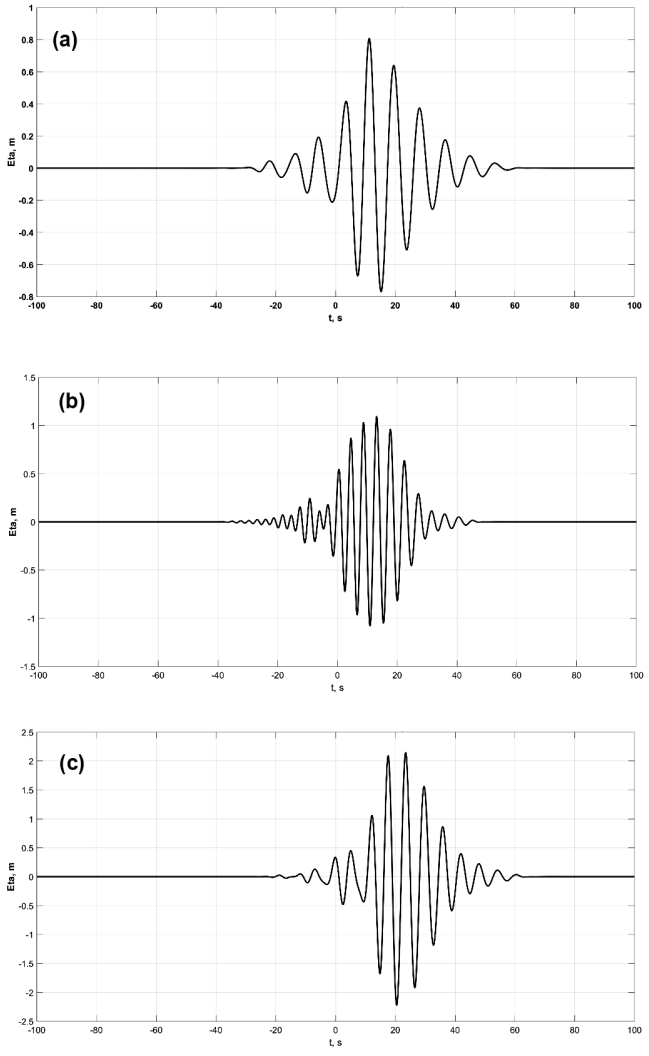

Figure 13. Imposed surface elevation at the generation boundary: **(a)** wave no. 1, **(b)** wave no. 3, **(c)** wave no. 4.

swap spectral shape with a peak enhancement factor equal to 3.3 is adopted, while the maximum wave height at the focusing point is identified through Goda's method (i.e. wave no. 1 $H_{\max} = 1.80$ m; wave no. 3 $H_{\max} = 3.24$ m; wave no. 4 $H_{\max} = 5.40$ m; Fig. 13); Goda (2000).

4.1.3 Grid generation

The domain mesh and prism layer grid are generated using the mesh generator in STAR-CCM+. Grid resolution is finer near the free surface and around the quay wall structure to capture both the wave dynamics and the details of the flow around the structure; Fig. 14. Prism-layer cells are generated along the structure's surface, and the height of the first layer is set so that the value of $y+$ (60 to 400) satisfies the turbulence model requirement by solving the velocity distribution outside the viscous sublayer, i.e. log-law regions are

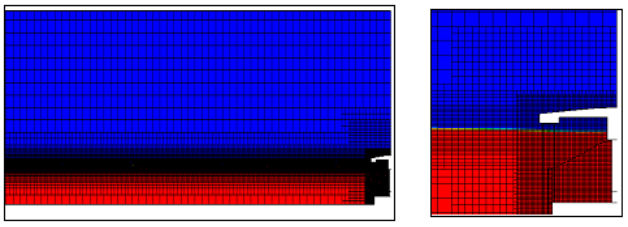

Figure 14. General domain grid and grid detail around the absorbing quay wall structure.

solved as presented in Demirel et al. (2014) and Schultz and Swain (2000). Regular hexahedral cells define the whole domain, while four thinner areas are used to capture free surface movements and the interaction between the wave group and the structure (V_{w1}, V_{w2}, V_{S1}, V_{S2}). The grid refinements across the water surface are realised by the volumetric controls, $V_{W1}$and V_{W2}, proposed along the whole domain. The size of V_{W2} is equal to the maximum simulated wave height, while the dimension of V_{W1} is 50 % larger (see longitudinal section in Fig. 14). V_{W2}'s horizontal grid size is determined according to the shortest generated wavelength (λ_{i1}) (i.e. $\Delta x = \Delta y = \lambda_{i1}/60$), while the vertical grid size is adjusted according to the smallest generated wave height (H_{i1}) ($\Delta z = H_{i1}/20$). Refinements around the structure present the same grid dimension of those used to discretized the water surface but their dimensions are set in order to include a gap between the structure surface and the volumetric control edges; the dimensions are equal to 1.0 m for V_{S1} and 5.0 m for V_{S2}. These mesh characteristics contribute to generating a grid of variable cell numbers from 2.0×10^6 to 3.5×10^6, according to the incident wave condition. To assure the numerical stability and to take the requested Courant number into account, a time step equal to $T_p/400$ is adopted in the study. All the RANS simulations are carried out on the work station at the hydraulic laboratory of the University of Bologna, using a double compute node consisting of hexa-core 2.00 GHz Intel Xeon E5. For a mesh made of 2.0×10^6 elements, it takes about 36 h on 12 cores to complete the entire wave group attack.

4.2 Results

The results are presented in terms of mean values of reflection coefficient (c_r) and pressures acting on the most significant parts of the structure. The pressure results are analysed only with respect to the extreme conditions. Surface elevation is measured through six wave gauges placed along the domain axis ($y = 0$) and at different distances from the quay wall (i.e. $x = -18; -16; -14; -12; -10; -8$ m). The gauge distances from the quay wall are at least $1/4$ of the peak wavelength in order to exclude the effects of stationary oscillations, which cannot be explained through the adopted reflection analysis method (Zelt and Skjelbreia, 1992).

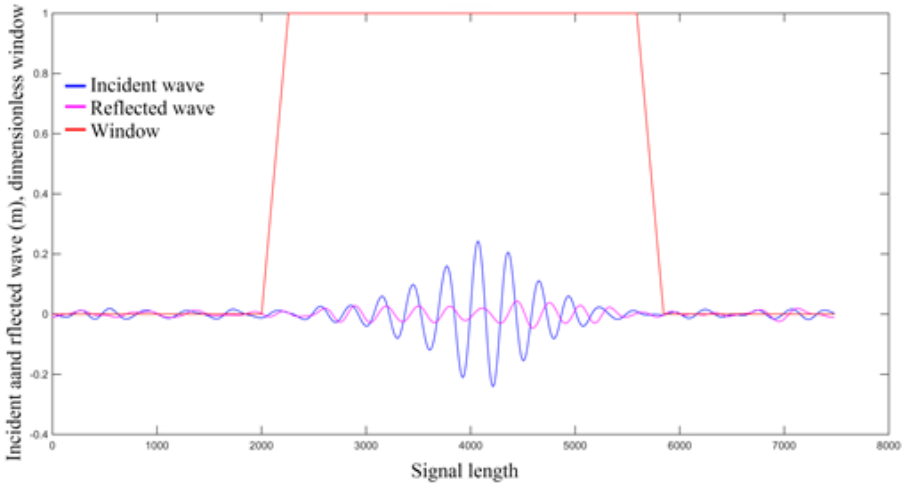

Figure 15. Example of the adopted window.

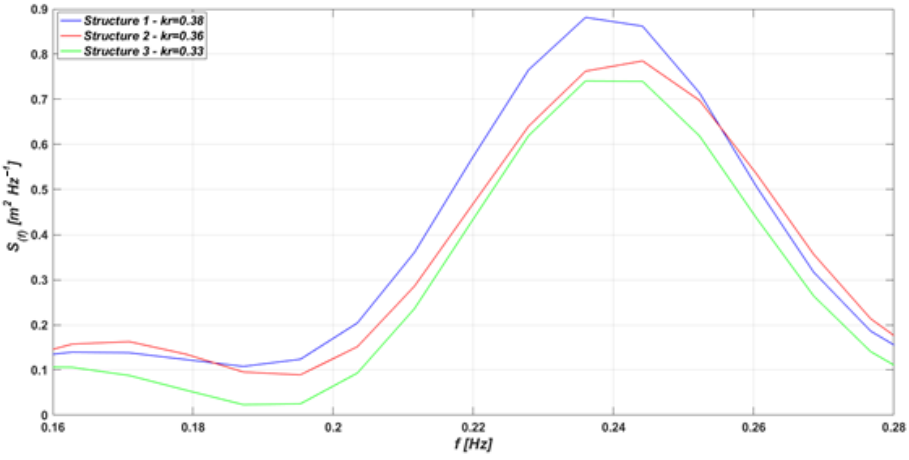

Figure 16. Comparison of reflected wave spectrums for wave no. 3.

4.2.1 Reflection coefficients results

Wave reflection induced by the quay wall is quantified by the reflection coefficient, defined as follows:

$$c_r = \frac{\sqrt{m_{0i}}}{\sqrt{m_{0r}}} = \frac{H_i}{H_r} \quad (2)$$

$$m_0 = \int_{0.5/f_p}^{1.5/f_p} S_{(f)} \cdot f^0 \cdot \mathrm{d}f, \quad (3)$$

where H_r and H_i are the reflected and incident wave heights, and m_{0r} and m_{0i} are the related zero-order spectral moments calculated between 0.5 and 1.5 times the peak frequency.

The calculation of the reflection coefficient is carried out through the spectral analysis of a non-stationary signal, since the generated wave group is represented by a short non-stationary time series. The approach implies the use of a time-fixed window (i.e. along the time series vector), centred on both incident and reflected wave groups. A trapezoidal-shaped window is used to reach this scope. Its length is defined according to the shape of the signal; i.e. the window begins with the first value above 0.05 m identified within the incident wave and closes after the last value above 0.05 m identified within the reflected signal. The window shape is characterised by two linear slopes between 0 and 1. The slope length is equal to 5 % of the group's envelope (Fig. 15). This approach is based on the assumption that the reflection phenomenon is linear, thus reflected and incident spectral shapes will not change except for the reduction of energy.

Figure 16 shows the comparison of the reflection coefficients for the three structures: it is clear that structure 3 is the best in terms of reducing the reflection. In fact it can be noticed that there is a generalized reduction of the reflected wave energy for whole range of analysed frequencies. With regard to the lower frequencies, i.e. incident wave periods

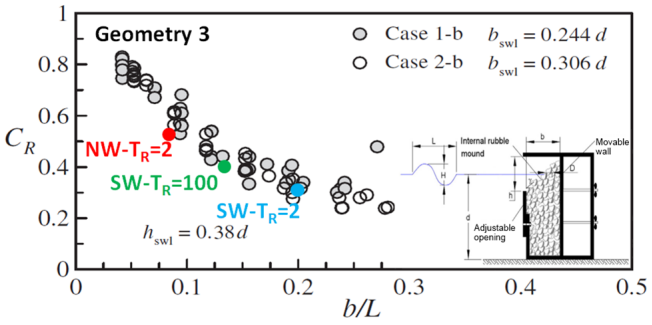

Figure 17. Comparison between physical results (Liu and Faraci, 2014) and CFD results for geometry 3, where b is absorbing chamber width, L is the wavelength, d is the water depth at the structure toe, h_{swl} is the submerged depth of the front wall, b_{swl} is the width of the surface piercing rubble mound at the still water.

longer than 4.5 s, the required wave attenuation cannot be guaranteed only by the resonance phenomenon of the cell. In this light the presence of the rocks inside the cell becomes more important. The arrangement of the geometry with the smaller armour slope (structure 2, red line in Fig. 16) does not induce the expected general improvement, whereas it becomes important for structure 3.

With regard to the higher frequencies with incident wave periods shorter than 4.5 s, the significant improvement associated with structure 3 is mainly due to the variable length of the absorbing cell generated by the inner slope that faces the incoming waves. With regard to the central frequencies, i.e. incident wave periods around 4.5 s, the largest improvement is between structures 1 and 2 because of the increased length of the absorbing cell. Structure 1 presents a ratio between its own length and wavelength equal to 0.18 while for structure 2 it is 0.195, facilitating the establishment of resonance conditions inside the cell. In order to validate the reflection coefficient results and highlight the capability of the numerical model to reproduce the dissipation due to the wave breaking on the rubble mound a comparison with the experimental results proposed by Liu and Faraci (2014) and Faraci et al. (2014) is presented in Fig. 17. The experiments, carried out at the Hydraulics Laboratory of the University of Messina, analysed a new combined caisson, including an open window on the front wall and an internal rubble mound with a slope. The caisson was made of steel and was composed by a double chamber in the wave crest direction and a vertical bulkhead in the front part. The inner part of the caisson was filled with rubble mound in order to simulate a rock armour. A comparison between the numerical solution and the experimental data is given in Fig. 17, in which it can be seen that the agreement between the CFD results and the experimental data is reasonable.

A synthesis of the reflection coefficients is presented in Table 5, in which we can consider the averaged reflection coefficient obtained for structure 3 to be satisfactory. Therefore, structure 3, presented in Fig. 10, has been selected as the optimum structure for the future quay wall of Vlorë Harbour.

Table 5. Calculated reflection coefficients.

Structure	Wave no.	Reflection coeff. (C_R)
Structure 1	Wave no. 3	0.38
Structure 2	Wave no. 3	0.36
Structure 3	Wave no. 3	0.33
Structure 3	Wave no. 1	0.56
Structure 3	Wave no. 4	0.40

Table 6. Calculated design loads.

Structure	Wave no.	Pressure–force
Uplift frontal pressure	Wave no. 3	28.5 kPa
Uplift internal pressure	Wave no. 3	24.5 kPa
Frontal unitary force	Wave no. 3	17.0 kN m^{-1}
Sheet pile	Wave no. 3	Pressure profile described in Fig. 18d

4.2.2 Pressure results

This section presents the pressure and force values acting on different parts of the structure. In order to validate the numerical results, the forces acting on the upper structure are compared with the empirical results obtained according to McConnell's method (Fig. 18a, b, c, McConnell et al., 2004), whereas the pressure distribution on the front sheet pile is compared with the distribution calculated according to Goda's method (Goda, 2010); Fig. 18d.

Measurements of pressure were carried out using virtual pressure gauges: eight pressure gauges were used to measure the uplift pressure acting on the frontal beam (Fig. 18a), 20 pressure gauges were used to measure the uplift pressure acting on the internal beam (Fig. 18b), 4 pressure gauges were used to measure the horizontal unitary force acting on the frontal beam (Fig. 18c) and 16 pressure gauges were used to identify the pressure distribution on the frontal sheet pile (Fig. 18d).

Two main activities were carried out in order to reduce the effect of high-frequency loads and at the same time consider all wave gauges positioned on the investigated structure area. Firstly, the average pressure signal is calculated. Secondly, a low-band filter is applied with a cutting frequency equal to 2 Hz, which is roughly the natural period of the analysed structures. Then, the considered design pressure values are the maximum values of each filtered signal, while the pressure distribution on the frontal sheet pile is calculated according to the maximum value of each single-filtered pressure signal (Table 6).

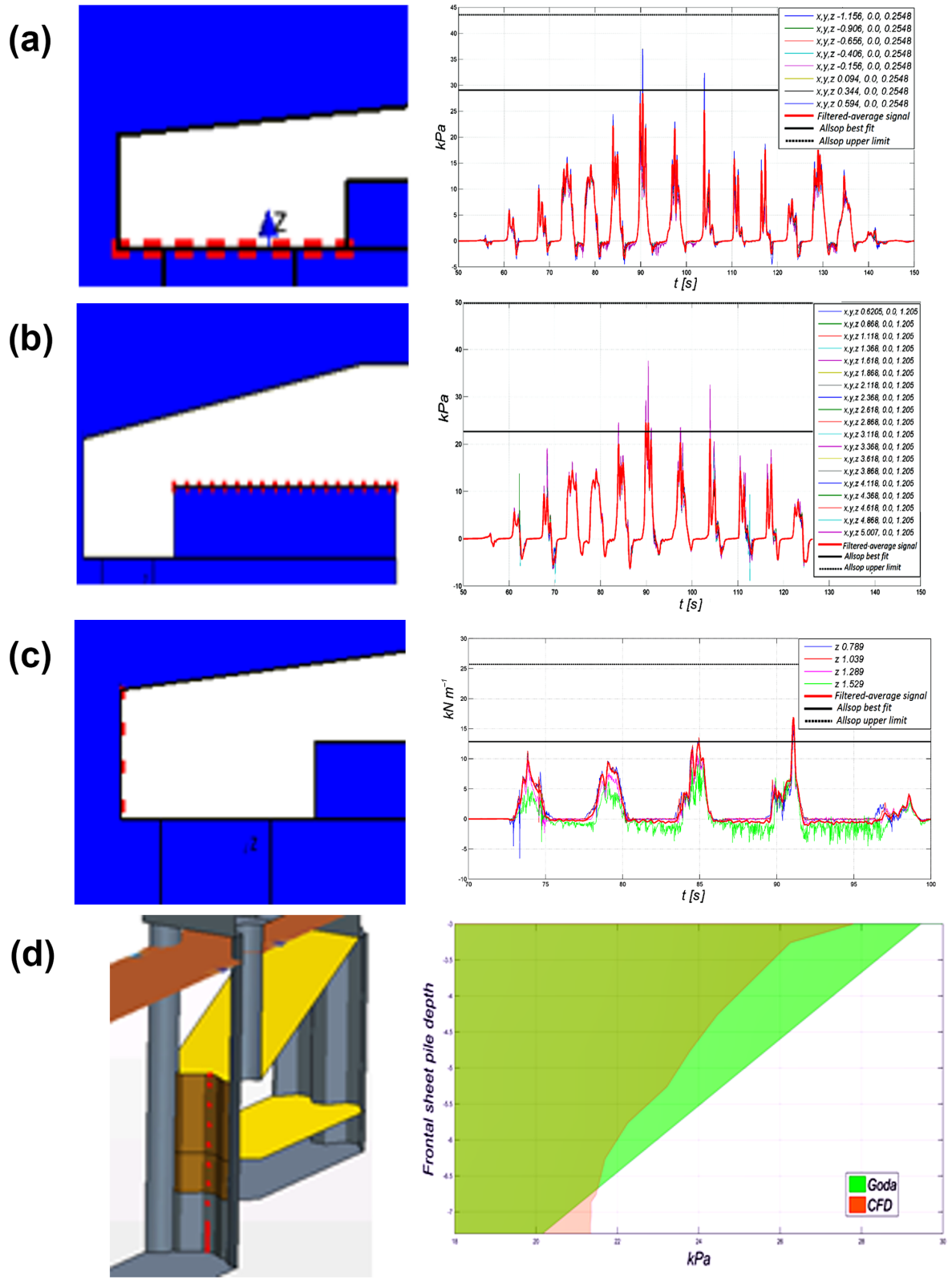

Figure 18. **(a, b, c)** Comparison between CFD results and empirical formulas proposed by McConnell et al. (2004) solid line refers to deterministic formula results while dotted line refers to probabilistic formula results. **(d)** Comparison between pressure distribution on the frontal sheet pile; orange refers to the CFD result and green refers to the well-known Goda's method.

5 Conclusion

This paper presents a study case in which the hindcasted wave data have been used to define the sea conditions with the aim of estimating the design wave states for an effective dock design based on an innovative quay wall concept.

Through a specific study case, the results provide a methodology, based on advanced numerical tools, to approach the design of coastal structures, focusing on the optimization of an innovative quay wall.

Design wave conditions are identified on the basis of the wind measurements and hindcasted wave data. Because of the different directions and periods, the identified wave conditions are distinguished in southerly and northerly waves. According to this classification two limit conditions were assessed: the limit of the exercise conditions for which the service condition has to be ensured, and the extreme limit for which the only requirement is the resistance of the structures. Once the wave conditions have been identified, the structure performance is analysed in terms of reflection coefficients by means of a CFD code. The optimisation of the absorbing cell is carried out only for the southerly wave conditions, while the complete reflection analysis is completed for the other two identified wave states. The resulting structure is a quay wall with an absorbing cell characterised by a ratio between its own length and wavelength equal to 0.195, filled with a 1 : 2 armour slope realised on the entire absorbing cell extension. The main findings are three values of reflection coefficients C_R 0.56, 0.33 and 0.4 for wave no. 1, 3 and 4. The result of the reflection coefficients, which is used to select the best design of the reflective quay wall, is also compared with experimental data in order to validate the numerical studies. The comparison shows a good agreement. With the same code the loads acting on the main structural parts of the quay wall are evaluated under the extreme southern conditions. Furthermore, a comparison of the numerical results with empirical formulas is proposed in order to validate the calculated pressure values. A general good agreement for the results is recognised through the compared pressure values. In conclusion sea data strongly supported the correct engineering design of the quay wall at Vlorë Harbour.

6 Data availability

The observational data used to carry out this research are free and available on request by writing to the authors.

Competing interests. The authors declare that they have no conflict of interest.

Acknowledgements. The authors gratefully acknowledge Giovanni Besio and Carlo Zumaglini, SIAP-MICROS s.r.l., for providing waves and wind data, and Piacentini, Ingegneri s.r.l., for the discussion on the quay design. Italian Flagship Project Ritmare IV (SP3_LI3_WP1) is gratefully acknowledged for partially supporting the research.

Edited by: I. Federico
Reviewed by: L. Martinelli and one anonymous referee

References

Altomare, C. and Gironella, X.: An experimental study on scale effects in wave reflection of low reflective quay walls with internal rubble mound for regular and random waves, Coast. Eng., 90, 51–63, doi:10.1016/j.coastaleng.2014.04.002, 2014.

Antonini, A., Lamberti, A., Archetti, R., and Miquel, A. M.: CFD investigations of OXYFLUX device, an innovative wave pump technology for artificial downwelling of surface water, Appl. Ocean Res., 61, 16–31, doi:10.1016/j.apor.2016.10.002, 2016a.

Antonini, A., Lamberti, A., Archetti, R., and Miquel, A. M.: Dynamic overset rans simulation of a wave-driven device for the oxygenation of deep layers, Ocean Eng., 127, 335–348, doi:10.1016/j.oceaneng.2016.10.016, 2016b.

Antonini, A., Tedesco, G., Lamberti, A., Archetti, R., Ciabattoni, S., and Piacentini, L.: Innovative combiwall quay-wall with internal rubble mound chamber: numerical tools supporting design activities, The case of Vlora's harbor, Proceeding of 26th International Ocean and Polar Engineering Conference, ISOPE 2016, Rhodos, 26 June–1 July 2016c.

Battjes, J. A. and Janssen, J. P. F. M.: Energy loss and Set-up due to breaking of random Waves, Proceeding of the 16th Int. Conf. On Coastal engineering, ASCE, 569–587, 27 August–3 September 1978.

Belu, R. and Koracin, D.: Wind characteristics and wind energy potential in western Nevada, Renew. Energ., 34, 2246–2251, doi:10.1016/j.renene.2009.02.024, 2009.

Boccotti, P.: Some new results on statistical properties of wind waves, Appl. Ocean Res., 5, 134–140, doi:10.1016/0141-1187(83)90067-6, 1983.

Boccotti, P.: Design waves and risk analysis, Elsevier Oceanography Series, Vol. 64, Wave mechanics for ocean engineering, 207–247, doi:10.1017/S0022112093003714, 2000.

Boccotti, P., Barbaro, G., and Mannino, L. A.: Field experiment on the mechanics of irregular gravity waves, J. Fluid Mech., 252, 173–186, doi:10.1017/S0022112093003714, 1993.

Booij, N., Ris, R. C., and Holthuijsen, L. H.: A third-generation wave model for coastal Regions 2: Verification, J. Geophys. Res.-Oceans, 104, 7667–7682, doi:10.1029/1998JC900123, 1999.

Burharth, H. and Andersen, O.: On the one dimensional steady and unsteady porous flow equations, Coast. Eng., 24, 233–257, doi:10.1016/0378-3839(94)00025-S, 1995.

CD-Adapco:USER GUIDE STAR-CCM+ Version 10.02, London, 2013.

Cruz, E., Isobe, M., and Watanabe, A.. Boussinesq equations for wave transformation on porous flow equations, Coast. Eng., 30, 125–154, doi:10.1016/S0378-3839(96)00039-7, 1997.

Demirel, Y. K., Khorasanchi, M., Turan, O., Incecik, A., and Schultz, M. P.: A CFD model for the frictional resistance prediction of antifouling coatings, Ocean Eng., 89, 21–31, 2014.

DHI: MIKE 21 SW. Spectral Wave Module. Scientific documentation, Hørsholm, DHI Water & Environment, 2011.

Eldeberky, Y. and Battjes, J. A.: Spectral modelling of wave breaking: Application to Boussinesq equations, J. Geophys. Res.-Oceans, 101, 1253–1264, 1996.

El-Hawary, F.: The Ocean Eng. Handbook, CRC Press, Taylor & Francis Group, ISBN-13: 9780849385988, CAT# 8598, 2000.

Engelund, F.: On the laminar and turbulent flows of ground water through homogeneous sand, Danish academy of Technical sciences, Koebenhavn, Akademie for de tekniske videnskaber, 1953.

Faraci, C., Cammaroto, B., Cavallaro, L., and Foti, E.: Wave reflection generated by caissons with internal rubble mound of variable slope, Proc. of 33rd International Conference on Coast. Eng., 1–6 July 2012.

Faraci, C., Scandura, P., and Foti, E.: Reflection of Sea Waves by Combined Caissons, J. Waterway, Port, Coastal, Ocean Eng., 141, doi:10.1061/(ASCE)WW.1943-5460.0000275, 04014036, 2014.

Gaeta, M. G., Samaras, A. G., Federico, I., Archetti, R., Maicu, F., and Lorenzetti, G.: A coupled wave-3-D hydrodynamics model of the Taranto Sea (Italy): a multiple-nesting approach, Nat. Hazards Earth Syst. Sci., 16, 2071–2083, doi:10.5194/nhess-16-2071-2016, 2016.

Garcia-Espinel, J. D., Alvarez-Garcia-Luben, R., Gonzalez-Herrero, J. M., and Castro-Fresno, D.: Glass fiber-reinforced polymer caissons used for construction of mooring dolphins in Puerto del Rosario harbor (Fuerteventura, Canary Islands), Coast. Eng., 98, 16–25, doi:10.1016/j.coastaleng.2015.01.003, 2015.

Goda, Y.: Random Seas and Design of Maritime Structures, 2nd edition, World Scientifc Publishing Co., Singapore, ISBN-13: 978-981-4282-39-0, 2000.

Hasselmann, S., Sasselmann, K., Allender, J. H., and Barnett, T. P.: Computations and parameterizations of non-linear energy transfer in gravity wave spectrum. Part II: parameterisations of nonlinear energy transfer for applications in wave models, J. Phys. Oceanogr., 15, 1369–1377, 1985.

Janssen, P. A. E. M.: Wave-induced stress and the drag of airflow over sea waves, J. Phys. Oceanogr., 19, 745–754, 1989.

Janssen, P. A. E. M.: Quasi-linear theory of wind-wave generation applied to wave forecasting, J. Phys. Oceanogr., 21, 1631–1642, 1991.

Jarlan, G. E.: A perforated vertical breakwater, The Dock and Harbour Authority, 21, 394–398, 1961.

Lamberti, A., Antonini, A., and Ceccarelli, G.: What could happen if the parbuckling of Costa Concordia had failed: Analytical and CFD-based investigation of possible generated wave, Proc of 34rd International Conference on Coast. Eng., 16–20 June 2014.

Lamberti, A., Antonini, A., and Archetti, R.: New Vlora's harbour, analysis of the internal wave agitation, Internal report, University of Bologna, 2015.

Liu, Y. and Faraci, C.: Analysis of orthogonal wave reflection by a caisson with open front chamber filled with sloping rubble mound, Coast. Eng., 91, 151–163, doi:10.1016/j.coastaleng.2014.05.002, 2014.

Masina, M., Lamberti, A., and Archetti, R.: Coastal flooding: A copula based approach for estimating the joint probability of water levels and waves, Coast. Eng., 97, 37–52, doi:10.1016/j.coastaleng.2014.12.010, 2015.

Mathiesen, M., Goda, Y., Hawkes, P. J., Mansard, E., Martín, M. J., Peltier, E., Thompson, E. F., and Van Vledder, G.: Recommended practice for extreme wave analysis, J. Hydraul. Res., 32, 803–814, doi:10.1080/00221689409498691, 1994.

Matteotti, G.: The reflection coefficient of a wave dissipating quay wall, Dock and Harbour Authority, 71, 285–291, 1991.

Mazas, F., Kergadallan, X., Garat, P., and Hamm, L.: Applying POT methods to the Revised Joint Probability Method for determining extreme sea levels, Coast. Eng., 91, 140–150, 2014.

McConnell, K., Allsop, W., and Cruickshank, I.: Piers, jetties and related structures exposed to waves: Guidelines for hydraulic loading, HR Wallingford, Thomas Telford, London, 2004.

Medina, J. R., Gonzalez-Escriva, J. A., Fort, L., Martinez, S., Ponce de Leon, D., Manuel, J., Yagüe, D., Garrido, J., and Berruguete, A.: Vertical Maritime Structure with Multiple Chambers for Attenuation of Wave Reflection, International PCT/EP2010/068000, EPO, The Hague, 23 pp., 2010.

Mentaschi, L., Besio, G., Cassola, F. and Mazzino, A.: Performance evaluation of WavewatchIII in the Mediterranean Sea, Ocean Model., 90, 82–94, doi:10.1016/j.ocemod.2015.04.003, 2015a.

Mentaschi, L., Perez, J., Besio, G., Mendez, F., and Menendez, M.: Parameterization of unresolved obstacles in wave modeling: a source term approach, Ocean Model., 96, 93–102, doi:10.1016/j.ocemod.2015.05.004, 2015b.

Menter, F. R.: Two Equation Eddy Viscosity Turbulence Models For Engineering Applications, Aiaa, 32, 1598–1605, 1994.

Monbaliu, J., Padilla-Hernández, R., Hargreaves, J. C., Carretero-Albiach, J. C., Luo, W., Sclavo, M., and Günther, H.: The spectral wave model WAM adapted for applications with high spatial resolution, Coast. Eng., 41, 41–62, doi:10.1016/S0378-3839(00)00026-0, 2000.

Samaras, A. G., Gaeta, M. G., Miquel, A. M., and Archetti, R.: High-resolution wave and hydrodynamics modelling in coastal areas: operational applications for coastal planning, decision support and assessment, Nat. Hazards Earth Syst. Sci., 16, 1499–1518, doi:10.5194/nhess-16-1499-2016, 2016.

Sartini, L., Mentaschi, L., and Besio, G.: How an optimized meteocean modelling chain provided 30 years of wave hindcast statistics: the case of the Ligurian Sea, Proc. of the 23rd International Conference on Coast. Eng., Seoul, South Korea, 16–20 June 2014.

Sartini, L., Cassola, F., and Besio, G.: Extreme waves seasonality analysis: an application in the Mediterranean Sea, J. Geophys. Res.-Oceans, 120, 6266–6288, doi:10.1002/2015JC011061, 2015a.

Sartini, L., Mentaschi, L., and Besio, G.: Comparing different extreme wave analysis models for wave climate assessment along the Italian coast, Coast. Eng., 100, 1–10, doi:10.1016/j.coastaleng.2015.03.006, 2015b.

Schultz, M. P. and Swain, G. W.: The influence of biofilms on skin friction drag, Biofouling, 15, 129–139, 2000.

Schweizer, J., Antonini, A., Govoni, L., Gottardi, G., Archetti, R., Supino, E., Berretta, C., Casadei, C., and Ozzi, C.: Investigating the potential and feasibility of an offshore wind farm in the Northern Adriatic Sea, Appl. Energ., 177, 449–463, doi:10.1016/j.apenergy.2016.05.114, 2016.

The WAMDI Group: The WAM Model. A Third Generation Ocean Wave Prediction Model, J. Phys. Oceanogr., 18, 1775–1810, doi:10.1016/j.oceaneng.2015.01.011, 1988.

Tromans, P. S., Anatruk, A. H. R., and Hagemeijer, P.: New model for the kinematics of large ocean waves application as a design wave, Proc. International Offshore and Polar Engineering Conf., 64–71, 11–16 August 1991.

US Army corps of engineers: Department of the army, Shore protection manual, Washington DC, 1984.

Viselli, A. M., Forristall, G. Z., Pearce, B. R., and Dagher, H. J.: Estimation of extreme wave and wind design parameters for offshore wind turbines in the Gulf of Maine using a POT method, Ocean Eng., 104, 649–658, doi:10.1016/j.oceaneng.2015.04.086, 2015.

Zelt, J. and Skjelbreia, E.: Estimating incident and reflected wave fields using an arbitrary number of wave gauges, Proc of 23rd International Conference on Coast. Eng., 4–9 October 1992.